A Basic Study on Modelling and Range-Extension Control for Dual IM-PMSM Electric Vehicles

An-Toan Nguyen[1,4], Binh-Minh Nguyen[2], João Pedro F. Trovão[1,3], Minh C. Ta[1,*]
[1]Dept. of Electrical and Computer Engineering, Université de Sherbrooke, Sherbrooke, QC, J1K 2R1, Canada
[2]Dept. of Advanced Energy, the University of Tokyo, Tokyo, Japan
[3]Polytechnic of Coimbra, IPC-ISEC and INESC Coimbra, 3030-199 Coimbra, Portugal
[4]Faculty of Engineering and Technology, Quy Nhon University, Quy Nhon, Binh Dinh, Vietnam
[*]Corresponding author: Cao.Minh.Ta@USherbrooke.ca

***Abstract*—This paper proposes a model-based control system to extend the range of dual-motor all-wheel-drive electric vehicles (EVs) using different electric motors (EMs). By analyzing EM, wheel, and chassis dynamics, a cost function involving driving force distribution ratio and motor current is introduced to minimize input power. An optimal driving force distribution strategy is developed to minimize energy consumption, suitable for real-time execution on conventional EV electronic control units. Computer simulations demonstrate the effectiveness of this strategy in both constant speed and acceleration/deceleration modes.**

***Index Terms*—Electric vehicle, Dual-motor All-wheel drive, Energy efficiency optimization, Driving force distribution**

I. Introduction

Electric Vehicles (EVs) face several challenges, including limited range, charging time, battery cost, and weight. Among these, the range remains the primary concern, prompting extensive research into multi-motor powertrains for EVs [1]. A prominent configuration within this research is the dual-motor all-wheel-drive (DM-AWD) setup, which features electric motors (EMs) on the front and rear axles. This configuration offers several advantages: (1) the ability to switch between two-wheel and all-wheel drive for enhanced control, (2) maintaining safe operation during sudden motor failures, and (3) optimizing torque distribution to reduce energy use and improve drivability [2]. To extend the range of DM-AWD EVs, it is essential to efficiently distribute power to each motor, focusing on minimizing energy consumption. This paper introduces an Energy Management Strategy (EMS) for DM-AWD EVs aimed at achieving significant energy savings.

Previous torque distribution strategies for DM-AWD EVs, often based on simple rules [3], lack efficiency and robustness due to their reliance on engineering experience. While many strategies have been developed to optimize energy distribution, existing research still faces several challenges.

Firstly, current strategies typically focus on the global dynamics of the EV, such as velocity, acceleration, total torque and force of the EV, without adequately accounting for the local dynamics of the EMs and wheels, such as EM speed and current, driving force, and wheel slip ratio. An optimization framework using vehicle velocity, total traction force, and Dynamic Programming to train an adaptive network-based fuzzy inference system was presented in a recent study [4]. Another EMS based on transmission efficiency, velocity, and total torque of the EV was proposed to optimize gear ratio and torque distribution [5], but it neglected the dynamics of EMs and wheels, where slip ratio can significantly impact energy loss, particularly on low-friction roads [6].

Secondly, power consumption models generally focus on a single type of motor, whereas future EVs are expected to integrate different types of EMs to expand their operational speed range. For instance, a model-based range extension control system was introduced to optimize front and rear driving-braking force distributions considering wheel slip ratio and Permanent Magnet Synchronous Motor (PMSM) losses [7]. A double-layer EMS for multi-motor EVs, employing passivity-based strategies, was devised to distribute torque commands and flux currents efficiently, preventing wheel slip and ensuring safe and energy-efficient operation [1]. Vo-Duy et al. developed an optimal strategy based on EM efficiency maps to address wheel slip losses in DM-AWD EVs, although they did not leverage the different performance characteristics of diverse EM types on the same vehicle [6].

To address these issues, this paper proposes a driving force distribution strategy (DFDS) for minimizing the power consumption of DM-AWD EVs, with the following main contributions: (1) developing a comprehensive input power model for DM-AWD EVs featuring two different EMs—an induction motor (IM) and a PMSM—which accounts for the dynamics of the motors, wheels, and chassis; (2) linking global and local dynamics by integrating vehicle dynamics with wheel dynamics and connecting the inner and outer layers of the control architecture, specifically torque and current distribution.

The subsequent sections will cover the vehicle dynamics and energy model, followed by an introduction to the proposed DFDS. A case study will be presented to validate the strategy, and the paper will conclude with remarks and suggestions for future research.

II. Vehicle Dynamics and Energy Model

A. Configuration of the Studied Vehicle

The DM-AWD configuration of the studied EV is presented in Fig. 1. The studied EV utilizes two different EMs, with IM mounted on the front axle and PMSM mounted on the rear

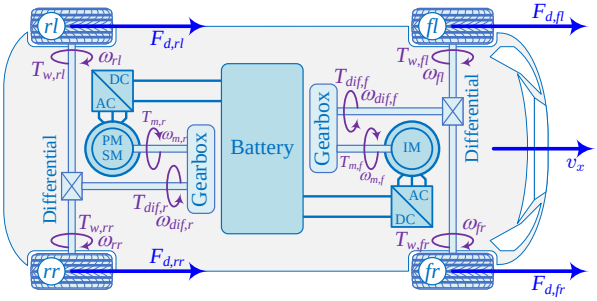

Fig. 1. Modelling of studied vehicle dynamics.

axle. To streamline the presentation of equations, the latter part of this paper will present variables and equations common to similar elements of the front and rear axles. Here, the subscript "i" denotes elements of both the front and rear axles, with "f" and "r" representing the front and rear axles, respectively. Additionally, this paper employs the subscript "j" to represent "l" and "r," corresponding to the variables of the left and right wheels of each axle, respectively. The main nomenclatures to describe the studied EV model are summarized in Table I. This paper only focuses on longitudinal motion, hence, the left and right driving force forces at each drivetrain are considered the same $F_{d,il} = F_{d,ir} = 0.5F_{d,i}$ and $\omega_{il} = \omega_{ir} = \omega_{w,i}$.

The DM-AWD configuration of the studied EVs offers several advantages. Firstly, it allows independent driving of the front and rear wheels, facilitating the distribution and control of torque for each motor based on driving conditions. Secondly, it enhances efficiency by expanding the speed range from low to high speeds compared to EVs with a single-drive motor by capitalizing on the high-efficiency working areas of these two different motors. Thirdly, the EV remains operational and safe even if one of the two motors fails while the vehicle is in motion. The strategy proposed in this paper aims to maximize the second advantage of this configuration.

B. Longitudinal Dynamics of the Studied Vehicle

Relationship between $\omega_{m,i}$ and $\omega_{w,i}$

$$\omega_{m,i} = G_i \omega_{w,i} \tag{1}$$

Equivalent dynamic equation of each motor

$$\widetilde{J}_{m,i}\dot{\omega}_{m,i} = T_{m,i} - r_w G_i^{-1} F_{d,i} \tag{2}$$

Slip ratio of the wheels

$$\lambda_i = \frac{r_w\omega_{w,i} - v_x}{max(r_w\omega_{w,i}, v_x, \varepsilon)} \tag{3}$$

In this study, the relationship between $F_{d,i}$ and λ_i is represented by the "magic formula" [8]

$$F_{d,i} = \mu_i Z_i \sin\left\{C \arctan\left[B\lambda_i - E\big(B\lambda_i - \arctan(B\lambda_i)\big)\right]\right\} \tag{4}$$

The driving force can be linearized if the slip ratio is small

$$F_{d,i} \simeq D_{s,i} Z_i \lambda_i \tag{5}$$

Where $D_{s,i}$ can be identified as outlined in [7].

The complete modelling and control of the studied EV have been presented in our publication [9].

TABLE I
NOMENCLATURE

Symbol	Description
Mechanical	
B, C, E	Shape coefficients of the magic formula
$D_{s,i}$	Driving stiffness coefficient of the each wheel
$F_{d,i}$	Total driving force of the front or rear wheels
$F_{d,ij}$	Driving force of each wheel
F_{tot}	Total driving force of the vehicle
G_i	Gear ratio on the front or rear drivetrain
$\widetilde{J}_{m,i}$	Equivalent rotational inertia moment of each motor
k_f	Driving force distribution ratio of the front wheels
$T_{m,i}$	Torque of IM or PMSM
v_x	Longitudinal velocity of the vehicle body
Z_i	Vertical force acting at the front or rear wheels
ε	Small positive value to avoid division by zero
λ_i	Slip ratio of the front or rear wheels
μ_i	Friction coefficient at the front or rear tires
ω_{ij}	Angular speed of each wheel
$\omega_{m,i}$	Mechanical angular speeds of IM or PMSM
$\omega_{w,i}$	Angular speed of the front or rear wheels
Electrical	
$C_{fe_{PM}}$	Iron loss coefficient of PMSM
$I_{d_{IM}}, I_{q_{IM}}$	d-q axes stator currents of IM
$I_{d_{PM}}, I_{q_{PM}}$	d-q axes stator currents of PMSM
$I_{dn_{IM}}$	Rated d-axis stator current of IM
$I_{max_{IM}}$	Maximum stator current magnitude of IM
$I_{max_{PM}}$	Maximum stator current magnitude of PMSM
$L_{d_{PM}}, L_{q_{PM}}$	d-q axes inductances of PMSM
$L_{m_{IM}}, L_{lr_{IM}}$	Magnetizing and rotor leakage inductances of IM
$L_{s_{IM}}, L_{r_{IM}}$	Stator and rotor inductances of IM
$p_{n_{IM}}, p_{n_{PM}}$	Number of pole pairs of IM and PMSM
$P_{cu_{IM}}, P_{fe_{IM}}$	Copper loss and iron loss of IM
$P_{cu_{PM}}, P_{fe_{PM}}$	Copper loss and iron loss of PMSM
$P_{m_{IM}}, P_{m_{PM}}$	Output powers of IM and PMSM
P_t	Total input power of the motors
V_{bat}	Battery voltage
r_w	Wheel radius
$R_{m_{IM}}$	Magnetizing resistance of IM
$R_{r_{IM}}$	Rotor resistance of IM
$R_{s_{IM}}, R_{s_{PM}}$	Stator resistance of IM and PMSM
ψ_{PM}	Permanent magnet rotor flux linkage of PMSM
$\omega_{e_{IM}}, \omega_{e_{PM}}$	Synchronous angular speed of IM and PMSM
$\omega_{sl_{IM}}$	Slip speed of IM

C. Power Model of the Motors

Output power, copper loss, iron loss, electromagnetic torque and electrical angular speed of IM [10]

$$P_{m_{IM}} = \omega_{m,f} T_{m,f} \tag{6}$$

$$P_{cu_{IM}} = R_{s_{IM}}(I_{d_{IM}}^2 + I_{q_{IM}}^2) + R_{r_{IM}} \frac{L_{m_{IM}}^2}{L_{r_{IM}}^2} I_{q_{IM}}^2 \tag{7}$$

$$P_{fe_{IM}} = \frac{\omega_{e_{IM}}^2 L_{m_{IM}}^2}{R_{m_{IM}}} \left(I_{d_{IM}}^2 + \frac{L_{lr_{IM}}^2}{L_{r_{IM}}^2} I_{q_{IM}}^2 \right) \tag{8}$$

$$T_{m,f} = 1.5 p_{n_{IM}} \cdot \frac{L_{m_{IM}}^2}{L_{r_{IM}}} I_{d_{IM}} I_{q_{IM}} \tag{9}$$

$$\omega_{e_{IM}} = p_{n_{IM}}\omega_{m,f} + \omega_{sl_{IM}} \simeq p_{n_{IM}}\omega_{m,f} + \frac{R_{r_{IM}}}{L_{r_{IM}}} \cdot \frac{I_{q_{IM}}}{I_{d_{IM}}} \tag{10}$$

Current and voltage constraints of IM

$$0 < I_{d_{IM}} \leq I_{dn_{IM}} \tag{11}$$

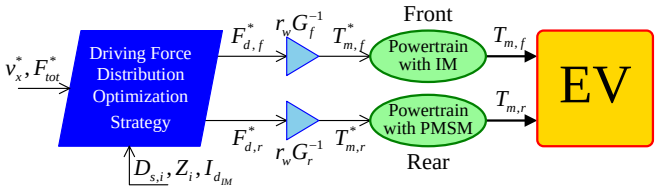

Fig. 2. Optimal driving force distribution scheme for DM-AWD EVs.

$$I_{d_{IM}}^2 + I_{q_{IM}}^2 \leq I_{max_{IM}}^2 \tag{12}$$

$$(\omega_{e_{IM}} L_{s_{IM}} I_{d_{IM}})^2 + (\omega_{e_{IM}} \sigma L_{s_{IM}} I_{q_{IM}})^2 \leq V_{max}^2 \tag{13}$$

where $\sigma = 1 - L_{m_{IM}}^2 / L_{s_{IM}} L_{r_{IM}}$, $V_{max} = V_{bat}/\sqrt{3}$

Output power, copper loss, iron loss, electromagnetic torque and electrical angular speed PMSM [10]

$$P_{m_{PM}} = \omega_{m,r} T_{m,r} \tag{14}$$

$$P_{cu_{PM}} = R_{s_{PM}} (I_{d_{PM}}^2 + I_{q_{PM}}^2) \tag{15}$$

$$P_{fe_{PM}} = C_{fe_{PM}} \omega_{e_{PM}}^{\varrho} \left\{ (\psi_{PM} + L_{d_{PM}} I_{d_{PM}})^2 + L_{q_{PM}}^2 I_{q_{PM}}^2 \right\} \tag{16}$$

$$T_{m,r} = 1.5 p_{n_{PM}} \cdot \left\{ \psi_{PM} I_{q_{PM}} + (L_{d_{PM}} - L_{q_{PM}}) I_{d_{PM}} I_{q_{PM}} \right\} \tag{17}$$

$$\omega_{e_{PM}} = p_{n_{PM}} \omega_{m,r} \tag{18}$$

where $\varrho = 1.5 \sim 1.6$

Current and voltage constraints of PMSM

$$-I_{f_{PM}} \leq I_{d_{PM}} \leq 0 \tag{19}$$

$$I_{d_{PM}}^2 + I_{q_{PM}}^2 \leq I_{max_{PM}}^2 \tag{20}$$

$$\omega_{e_{IM}}^2 L_{d_{PM}}^2 (I_{d_{PM}} + I_{f_{PM}})^2 + \omega_{e_{IM}}^2 L_{q_{PM}}^2 I_{q_{PM}}^2 \leq V_{max}^2 \tag{21}$$

where $I_{f_{PM}} = \psi_{PM} / L_{d_{PM}}$

The total input power model of the motors on the studied EV is equal to the sum of the power models above

$$P_t = P_{m_{IM}} + P_{m_{PM}} + P_{cu_{IM}} + P_{cu_{PM}} + P_{fe_{IM}} + P_{fe_{PM}} \tag{22}$$

III. Proposed Driving Force Distribution Strategy

A. Driving Force Distribution Scheme

Fig. 2 depicts the driving force distribution diagram that uses the proposed EMS to calculate $F_{d,f}^*$ and $F_{d,r}^*$ based on k_f, as described in Section III-C. Based on $F_{d,f}^*$ and $F_{d,r}^*$, the appropriate torques $T_{m,f}^*$ and $T_{m,r}^*$ are applied to the front and rear powertrains, respectively. Each powertrain includes a battery (shared), inverter, and EM equipped with current controllers and motor control strategies. Details of the control structure are fully presented in [9].

B. Energy Optimization Problem

Driving force at wheels

$$\begin{cases} F_{d,f} = k_f F_{tot} \\ F_{d,r} = (1 - k_f) F_{tot} \end{cases} \tag{23}$$

Where $0 \leq k_f \leq 1$. This means that if $k_f = 1$, F_{tot} of EV will be distributed entirely to the front IM. Conversely, if $k_f = 0$, F_{tot} will be distributed entirely to the rear PMSM.

From (2) and (23), the torque of each motor is approximated as

$$\begin{cases} T_{m_{IM}} \simeq \dfrac{r_w}{G_f} F_{d,f} = \dfrac{r_w}{G_f} k_f F_{tot} \\ T_{m_{PM}} \simeq \dfrac{r_w}{G_f} F_{d,r} = \dfrac{r_w}{G_f} (1 - k_f) F_{tot} \end{cases} \tag{24}$$

From (3), the angular speed of the wheel is approximated as

$$\omega_{w,i} \simeq \frac{v_x}{r_w} (1 + \lambda_i) \tag{25}$$

From (1) and (25), the angular speed of the motors is approximated as

$$\omega_{m,i} \simeq \frac{G_i v_x}{r_w} (1 + \lambda_i) \tag{26}$$

From (5), the slip ratio of the wheels is approximated as

$$\lambda_i \simeq \frac{F_{d,i}}{D_{s,i} Z_i} \tag{27}$$

From (9), (23) and (24), the q-axis current of IM is approximated as

$$I_{q_{IM}} \simeq \frac{k_{IM} k_f F_{tot}}{I_{d_{IM}}} \tag{28}$$

Where

$$k_{IM} = \frac{r_w L_{r_{IM}}}{1.5 p_{n_{IM}} L_{m_{IM}}^2 G_f} \tag{29}$$

From (17), (23) and (24), the q-axis current of PMSM is approximated as

$$I_{q_{PM}} \simeq \frac{k_{PM} (1 - k_f) F_{tot}}{\psi_{PM} + (L_{d_{PM}} - L_{q_{PM}}) I_{d_{PM}}} \tag{30}$$

Where

$$k_{PM} = \frac{r_w}{1.5 p_{n_{PM}} G_f} \tag{31}$$

The q-axis current of PMSM (30) is approximated as

$$I_{q_{PM}} \simeq \frac{k_{PM} (1 - k_f) F_{tot}}{\psi_{PM}} \tag{32}$$

Assuming the slip ratio is small, from (10) and (18) we can approximate the electrical angular speed of the motors as

$$\begin{cases} \omega_{e_{IM}} \simeq \dfrac{p_{n_{IM}} G_f v_x}{r_w} + \dfrac{R_{r_{IM}}}{L_{r_{IM}}} \cdot \dfrac{I_{q_{IM}}}{I_{d_{IM}}} \\ \omega_{e_{PM}} \simeq \dfrac{p_{n_{PM}} G_r v_x}{r_w} \end{cases} \tag{33}$$

Substitute (28) for (33), the electrical angular speed of IM is approximated as

$$\omega_{e_{IM}} \simeq \frac{p_{n_{IM}} G_f v_x}{r_w} + \frac{R_{r_{IM}} k_{IM} k_f F_{tot}}{L_{r_{IM}} I_{d_{IM}}^2} \tag{34}$$

1) Power Model of IM: Substitute (24) and (26) for (6) into (35). Then, substitute (28) for (7) into (36). Next, substitute (28) and (34) for (8) into (37).

$$\widetilde{P}_{m_{IM}} = v_x \left(k_f F_{tot} + \frac{k_f^2 F_{tot}^2}{D_{s,f} Z_f} \right) \tag{35}$$

$$\widetilde{P}_{cu_{IM}} = R_{s_{IM}} \left(I_{d_{IM}}^2 + \frac{k_{IM}^2 k_f^2 F_{tot}^2}{I_{d_{IM}}^2} \right) + \frac{R_{r_{IM}} L_{m_{IM}}^2 k_{IM}^2 k_f^2 F_{tot}^2}{L_{r_{IM}}^2 I_{d_{IM}}^2} \tag{36}$$

$$\widetilde{P}_{fe_{IM}} = \frac{L_{m_{IM}}^2}{R_{m_{IM}}} \left\{ \begin{array}{l} \left(I_{d_{IM}}^2 + \dfrac{L_{lr_{IM}}^2 k_{IM}^2 k_f^2 F_{tot}^2}{L_{r_{IM}}^2 I_{d_{IM}}^2} \right) \\ \cdot \left(\dfrac{p_{n_{IM}} G_f v_x}{r_w} + \dfrac{R_{r_{IM}} k_{IM} k_f F_{tot}}{L_{r_{IM}} I_{d_{IM}}^2} \right)^2 \end{array} \right\} \tag{37}$$

To represent the current and voltage constraints of the IM, substitute (12) into (38) using (28) and substitute (13) into (39) using (28) and (34)

$$I_{d_{IM}}^2 + \left(\frac{k_{IM} k_f F_{tot}}{I_{d_{IM}}} \right)^2 \leq I_{max_{IM}}^2 \tag{38}$$

$$\left\{ \begin{array}{l} L_{s_{IM}}^2 \left(\dfrac{p_{n_{IM}} G_f v_x}{r_w} + \dfrac{R_{r_{IM}} k_{IM} k_f F_{tot}}{L_{r_{IM}} I_{d_{IM}}^2} \right) \\ \cdot \left[I_{d_{IM}}^2 + \left(1 - \dfrac{L_{m_{IM}}^2}{L_{s_{IM}} L_{r_{IM}}} \right)^2 \left(\dfrac{k_{IM} k_f F_{tot}}{I_{d_{IM}}} \right)^2 \right] \end{array} \right\} \leq \frac{V_{bat}^2}{3} \tag{39}$$

2) Power Model of PMSM: Substitute (24) and (26) for (14) into (40). Then, substitute (32) for (15) into (41). Next, substitute (32) and (33) for (16) into (42).

$$\widetilde{P}_{m_{PM}} = v_x \left\{ (1 - k_f) F_{tot} + \frac{(1 - k_f)^2 F_{tot}^2}{D_{s,r} Z_r} \right\} \tag{40}$$

$$\widetilde{P}_{cu_{PM}} = R_{s_{PM}} \left\{ I_{d_{PM}}^2 + \left(\frac{k_{PM} (1 - k_f) F_{tot}}{\psi_{PM}} \right)^2 \right\} \tag{41}$$

$$\begin{aligned} \widetilde{P}_{fe_{PM}} = \; & C_{fe_{PM}} \left(\frac{p_{n_{PM}} G_r v_x}{r_w} \right)^{\varrho} \\ & \cdot \left\{ \begin{array}{l} (\psi_{PM} + L_{d_{PM}} I_{d_{PM}})^2 \\ + \left(\dfrac{L_{q_{PM}} k_{PM} (1 - k_f) F_{tot}}{\psi_{PM}} \right)^2 \end{array} \right\} \end{aligned} \tag{42}$$

To represent the current and voltage constraints of the PMSM, substitute (20) into (43) using (32) and substitute (21) into (44) using (32) and (33)

$$I_{d_{PM}}^2 + \left(\frac{k_{PM} (1 - k_f) F_{tot}}{\psi_{PM}} \right)^2 \leq I_{max_{PM}}^2 \tag{43}$$

$$\left(\frac{p_{n_{PM}} G_r v_x}{r_w} \right)^2 \left\{ \begin{array}{l} L_{d_{PM}}^2 (I_{d_{PM}} + I_{f_{PM}})^2 \\ + \left(\dfrac{L_{q_{PM}}^2 k_{PM} (1 - k_f) F_{tot}}{\psi_{PM}} \right)^2 \end{array} \right\} \leq \frac{V_{bat}^2}{3} \tag{44}$$

3) Input Power Model: Summing the above power models, the total input power model of the motors on the studied EV is equal to

$$\begin{aligned} \widetilde{P}_t \; &= \; \widetilde{P}_{m_{IM}} + \widetilde{P}_{m_{PM}} + \widetilde{P}_{cu_{IM}} + \widetilde{P}_{cu_{PM}} + \widetilde{P}_{fe_{IM}} + \widetilde{P}_{fe_{PM}} \\ &= \; \Im_1 \frac{k_f^4}{I_{d_{IM}}^6} + \Im_2 \frac{k_f^3}{I_{d_{IM}}^4} + \Im_3 \frac{k_f^2}{I_{d_{IM}}^2} + \Im_4 k_f^2 - \Im_5 k_f \\ &\quad + \Im_6 I_{d_{IM}^2} + \Im_7 I_{d_{PM}^2} + \Im_8 I_{d_{PM}} + \Im_9 \end{aligned} \tag{45}$$

Where $\Im_1 \sim \Im_9$ are the coefficients containing parameters of the studied motors and variables v_x, F_{tot}, $D_{s,i}$ and Z_i.

4) Optimization Problem: To generate a specific F_{tot} for a given v_x, there are many possible sets of $(k_f, I_{d_{IM}}, I_{d_{PM}})$ numbers. However, one may consider the set $(k_f, I_{d_{IM}}, I_{d_{PM}})$ that minimizes the input power $\widetilde{P}_t$ for a given F_{tot} and v_x, while adhering to constraints related to the driving force distribution ratio, voltages, and currents.

$$\begin{aligned} & \min_{\{k_f, I_{d_{IM}}, I_{d_{PM}}\}} \widetilde{P}_t = \text{Eq. (45)} \\ & \text{s.t. } 0 \leq k_f \leq 1, (11), (19), (38), (39), (43), (44) \end{aligned} \tag{46}$$

Because the input power minimization problem is an optimization problem under inequality constraints, one may apply the Kuhn-Tucker theorem to calculate the optimal values of $(k_f, I_{d_{IM}}, I_{d_{PM}})$. However, this paper proposes a simpler optimal solution that still ensures minimization of the input power of EMs in sections III-C.

C. Optimal solution for input power minimization

In this paper, the efficiency of the inverters is assumed to be constant. Thus, the focus of this problem is solely on minimizing the input power of the two drive motors (IM and PMSM) to reduce battery power consumption. This is achieved by determining the optimal driving force distribution ratio for the front wheels, denoted as $k_{f_{opt}}$. Subsequently, based on $k_{f_{opt}}$, the appropriate required torques are assigned to the two motors, as depicted in Fig. 2, to enhance global efficiency. The strategy for calculating $k_{f_{opt}}$ will be presented in detail below.

Because $k_f = 0 \sim 1$ very small compared to $I_{d_{IM}}$, the terms such as $\frac{k_f^4}{I_{d_{IM}}^6}$ and $\frac{k_f^3}{I_{d_{IM}}^4}$ in (45) are almost zero. Hence, by removing the terms with high-order components in (45), the total input power model can be rewritten to the reduced second-order polynomial

$$\begin{aligned} \widetilde{P}_t \simeq & \left(\frac{\Im_3}{I_{d_{IM}}^2} + \Im_4 \right) k_f^2 - \Im_5 k_f \\ & + \Im_6 I_{d_{IM}^2} + \Im_7 I_{d_{PM}^2} + \Im_8 I_{d_{PM}} + \Im_9 \end{aligned} \tag{47}$$

Assuming that v_x, F_{tot}, $D_{s,i}$, Z_i, $I_{d_{IM}}$ and $I_{d_{PM}}$ remain constant in the static state of the system, the optimization problem (46) becomes a simpler optimization problem (48).

$$\begin{aligned} & \min_{\{k_f\}} \widetilde{P}_t = \text{Eq. (47)} \\ & \text{s.t. } 0 \leq k_f \leq 1 \end{aligned} \tag{48}$$

The minimization condition $\widetilde{P}_t$ concerning k_f is given by

$$\left.\frac{\partial \widetilde{P}_t}{\partial k_f}\right|_{v_x, F_{tot}, D_{s,i}, Z_i, I_{d_{IM}}, I_{d_{PM}}} = 0 \tag{49}$$

Using (47), condition (49) is satisfied when

$$2\left(\frac{\Im_3}{I_{d_{IM}}^2} + \Im_4\right) k_f - \Im_5 = 0 \tag{50}$$

Therefore, the total power minimization condition for the studied EV is given by

$$k_{f_{opt}} = \frac{0.5\Im_5 I_{d_{IM}}^2}{\Im_3 + \Im_4 I_{d_{IM}}^2} \tag{51}$$

After implementing the $\Im_3$, $\Im_4$ and $\Im_5$ coefficients in detail, the value of k_f is calculated based on (52).

IV. Simulation for Comparative Evaluation

A. Simulation Setting

The proposed DFDS is validated in the MATLAB/Simulink® environment to evaluate the performance of the strategy for DM-AWD EVs. The parameters of the studied vehicle are listed in Table II, and its modelling is described in [9]. The reference velocity of the EV follows the driving cycle WLTC class 2 (WLTC2) with road friction coefficient $\mu = 0.87$.

B. Results and Discussion

Fig. 3 shows that the vehicle fully meets the required velocity according to the WLTC2. In this result, the optimal distribution value $k_{f_{opt}}$ (52) is utilized to distribute the driving force, as depicted in Fig. 2. This result validates that the proposed strategy has appropriately applied the necessary torque value to the two motors.

Because the proposed strategy relies heavily on approximations to obtain $\widetilde{P}_t$ (47), the results shown in Fig. 4 aim to demonstrate the accuracy of $\widetilde{P}_t$ (47). This analysis is conducted using WLTC2 and $k_f = 0.5$. The comparison results indicate that the difference between $\widetilde{P}_t$ (47) and P_t (22) is minimal in the vehicle speed range below 25 km/h, but it increases as the vehicle speed surpasses 25 km/h. While significant differences are observed in the high-speed region, all values of P_t (22) consistently exceed those of $\widetilde{P}_t$ (47). Thus, if $\widetilde{P}_t$ (47) is reduced by the proposed strategy, P_t (22) must decrease accordingly. These results align with the objectives of this paper.

TABLE II
Physical Parameters of e-Commander Platform

Parameter		Value
Vehicle		
Equivalent vehicle mass	m	857 kg
Height of the center of gravity	h_{CG}	0.585 m
Distance of front axle from CG	l_f	0.865 m
Distance of rear axle from CG	l_r	1.058 m
Front wheels track width of the vehicle	d_f	1.257 m
Rear wheels track width of the vehicle	d_r	1.219 m
Gear ratio on the front drivetrain	G_f	6.75
Gear ratio on the rear drivetrain	G_r	12.25
Effective radius of tire	r_w	0.318 m
Equivalent inertia moment of the wheel	$\widetilde{J}_{\omega,i}$	0.55 kgm^2
Drag coefficient	c_d	0.65
Equivalent frontal area	A_x	2 m^2
Front Motor (IM)		
Stator resistance	$R_{s_{IM}}$	1.627 mΩ
Rotor resistance	$R_{r_{IM}}$	0.415 mΩ
Magnetizing inductance	$L_{m_{IM}}$	320 μH
Rotor leakage inductance of IM	$L_{lr_{IM}}$	19.42 μH
Rotor inductance	$L_{r_{IM}}$	339.42 μH
Number of pole pairs	$p_{n_{IM}}$	2
Rear Motor (PMSM)		
Stator resistance	$R_{s_{PM}}$	0.985 mΩ
Iron loss coefficient	$C_{fe_{PM}}$	0.021
Nominal d-axis inductance	$L_{d_{PM}}$	15.02 μH
Nominal q-axis inductance	$L_{q_{PM}}$	29.75 μH
Permanent magnet rotor flux linkage	ψ_{PM}	0.03 Wb
Number of pole pairs	$p_{n_{PM}}$	2
Batteries		
Battery bank capacity	C_{bat}	110 Ah
Battery bank resistance (at 80% SoC)	R_{bat}	6 mΩ
No. of modules in series	N_s	4
No. of modules in parallel	N_p	3

e-Commander Platform at e-TESC Lab

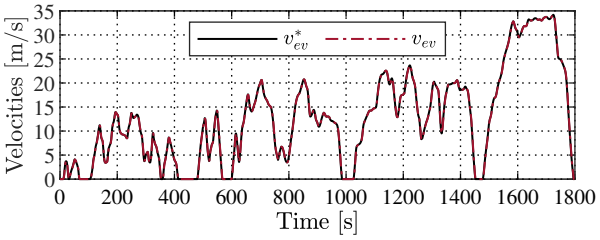

Fig. 3. Velocity responses of the proposed EMS with WLTC2.

$$k_{f_{opt}} = \frac{\left\{\frac{F_{tot}^2 v_x}{D_{s,r} Z_r} - \frac{p_{n_{IM}} R_{r_{IM}} L_{m_{IM}}^2 k_{IM} F_{tot} G_f v_x}{R_{m_{IM}} L_{r_{IM}} r_w} + \frac{R_{s_{PM}} k_{PM}^2 F_{tot}^2}{\psi_{PM}^2} + \frac{C_{fe_{PM}} L_{q_{PM}}^2 k_{PM}^2 F_{tot}^2 \left(\frac{p_{n_{PM}} G_r v_x}{r_w}\right)^{\varrho}}{\psi_{PM}^2}\right\} I_{d_{IM}}^2}{\left\{\begin{array}{l}\left(\frac{R_{r_{IM}} L_{m_{IM}}^2}{L_{r_{IM}}^2} + \frac{R_{r_{IM}}^2 L_{m_{IM}}^2}{R_{m_{IM}} L_{r_{IM}}^2} + \frac{p_{n_{IM}}^2 L_{m_{IM}}^2 L_{lr_{IM}}^2 G_f^2 v_x^2}{R_{m_{IM}} L_{r_{IM}}^2 r_w^2} + R_{s_{IM}}\right) k_{IM}^2 F_{tot}^2 \\ + \left[\frac{v_x}{D_{s,f} Z_f} + \frac{v_x}{D_{s,r} Z_r} + \frac{R_{s_{PM}} k_{PM}^2}{\psi_{PM}^2} + \frac{C_{fe_{PM}} L_{q_{PM}}^2 k_{PM}^2 \left(\frac{p_{n_{PM}} G_r v_x}{r_w}\right)^{\varrho}}{\psi_{PM}^2}\right] F_{tot}^2 I_{d_{IM}}^2\end{array}\right\}} \tag{52}$$

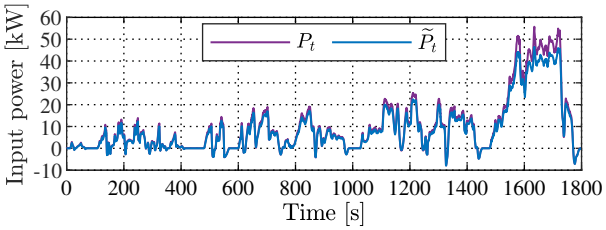

Fig. 4. Comparison of the motor powers.

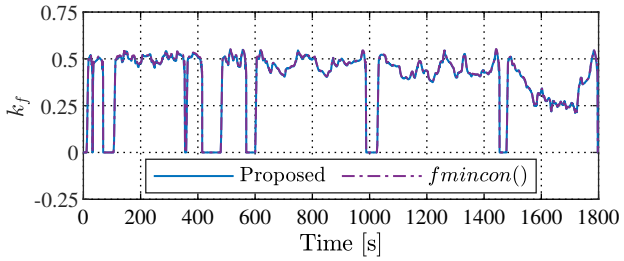

Fig. 5. Comparison of the distribution ratio.

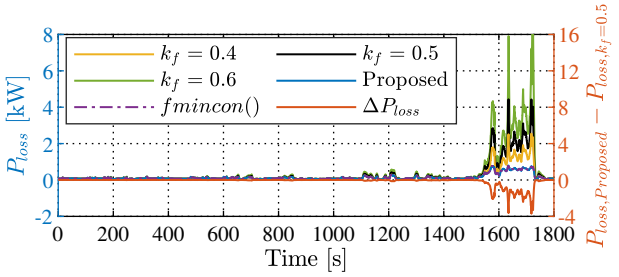

Fig. 6. Compare the power loss of the strategies.

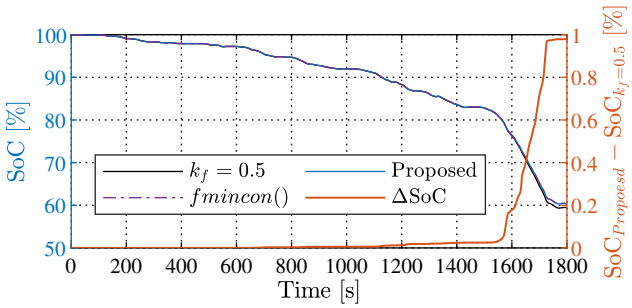

Fig. 7. Comparison of the battery SoC with WLTC2 driving cycle.

To assess the optimal value of $k_{f_{opt}}$ (52), the result obtained from $k_{f_{opt}}$ (52) is compared with the result of calculating k_f using the optimal value calculation function $fmincon()$ of MATLAB/Simulink®. Both calculations of $k_{f_{opt}}$ with (52) and using $fmincon()$ follow WLTC2. However, to evaluate the accuracy of $k_{f_{opt}}$ (52), the process of calculating k_f with $fmincon()$ utilizes the cost function $\widetilde{P}_t$ (45), which does not remove high-order components. The results presented in Fig. 5 indicate that the calculation of $k_{f_{opt}}$ using (52) does not significantly differ from k_f calculated using $fmincon()$. This demonstrates the accuracy and optimality of the optimal value $k_{f_{opt}}$ according to (52) of the proposed strategy.

Fig. 6 and 7 show the capability of the proposed strategy to decrease energy consumption. Fig. 6 illustrates that the total power loss of EMs P_{loss} when employing the proposed strategy is consistently lower than that of the method with k_f = const. Furthermore, P_{loss} when using the proposed strategy is significantly lower than the method with k_f = const in high-speed regions (> 25 km/h). Fig. 7 further demonstrates that the reduction in battery State of Charge (SoC) using the proposed strategy is less than that of the method with $k_f = 0.5$. In summary, despite relying on numerous approximations and simple calculations, the proposed strategy effectively reduces the power consumption of EVs.

V. Conclusion

This paper proposes a model-based range extension control strategy for DM-AWD EVs, with a focus on optimizing driving force distribution for front and rear wheels. Utilizing the dynamics of the EMs, wheels, and chassis, we introduce an input power model for dual IM-PMSM EVs, applied as a cost function to minimize energy consumption. Subsequently, we present a simple yet effective strategy for optimizing traction distribution in DM-AWD EVs. Simulation test results demonstrate the efficacy of this novel strategy in extending the cruising range of DM-AWD EVs. While this paper specifically addresses the optimization of driving force distribution ratios, future work will concentrate on validating the proposed strategy on e-Commander platform at e-TESC Lab.

References

[1] B.-M. Nguyen, J. P. F. Trovão, and M. C. Ta, "Double-Layer Energy Management for Multi-Motor Electric Vehicles," IEEE Trans. Veh. Technol., vol. 72, no. 7, pp. 8623-8635, 2023.

[2] N. Mutoh and Y. Nakano, "Dynamics of Front-and-Rear-Wheel-Independent-Drive-Type Electric Vehicles at the Time of Failure," IEEE Trans. Ind. Electron., vol. 59, no. 3, pp. 1488-1499, 2012.

[3] S. De Pinto *et al.*, "Torque-Fill Control and Energy Management for a Four-Wheel-Drive Electric Vehicle Layout With Two-Speed Transmissions," IEEE Trans. Ind. Appl., vol. 53, no. 1, pp. 447-458, 2018.

[4] C. T. P. Nguyen *et al.*, "Torque Distribution Optimization for a Dual-Motor Electric Vehicle Using Adaptive Network-Based Fuzzy Inference System," IEEE Trans. Energy Convers., vol. 38, no. 4, 2023.

[5] J. Wang *et al.*, "Drive-Cycle-Based Configuration Design and Energy Efficiency Analysis of Dual-Motor 4WD System With Two-Speed Transmission for Electric Vehicles," IEEE Trans. Transp. Electrif., vol. 10, no. 1, pp. 1887–1899, 2024.

[6] T. Vo-Duy *et al.*, "Optimal Energy Management System of Dual-motor Electric Vehicles with Longitudinal Dynamic Characteristic Consideration," IEEE Trans. Veh. Technol., 2023.

[7] H. Fujimoto and S. Harada, "Model-Based Range Extension Control System for Electric Vehicles With Front and Rear Driving–Braking Force Distributions," IEEE Trans. Ind. Electron., vol. 62, no. 5, 2015.

[8] H. B. Pacejka, Tire and Vehicle Dynamics, 3rd ed., Elsevier, 2006.

[9] A.-T. Nguyen, B.-M. Nguyen, J. P. F. Trovao, and C. M. Ta, "Modelling and Control of Dual-motor All-Wheel Drive Electric Vehicles Using Energetic Macroscopic Representation," Prog. Can. Mech. Eng., 2023.

[10] K. Hee Nam, AC Motor Control and Electrical Vehicle Applications, CRC Press, 2010.